Journal of Materials and Environmental Sciences
ISSN : 2028-2508

JMES, 2017 Volume 8, Issue 7, Page 2428-2441

http://www.jmaterenvironsci.com /

Electrochemical and quantum chemical study of 1-ethyl-1H-pyrazolo [3, 4-d] pyrimidine-4(5H)-thione as corrosion inhibitor for mild steel in HCl solution

L. El Hattabi[1]*, S. Echihi[1,3], M. El Fal[2], A. Guenbour[1], Y. Ramli[4], E.M. Essassi[2], M. Tabyaoui[1]

[1]*Laboratory of Nanotechnology, Materials and Environment, Department of Chemistry, Faculty of Science, University Mohammed V. Av, Ibn Batouta, BP, 1014 Rabat. Morocco*

[2]Laboratory Organic Chemistry Heterocyclic *URAC 21*, Cluster Competence Pharmacochemistry, *Faculty of Science, University Mohammed V. Av, Ibn Batouta, BP, 1014 Rabat. Morocco*

[3]*Laboratory of Water and Environment, Faculty of Sciences of El jadida, BP 20, 24000 El jadida. Morocco*

[4]*Medicinal Chemistry Laboratory, Faculty of Medicine and Pharmacy, Mohammed V University, Rabat. Morocco.*

Received 29 May 2016,
Revised 19 Dec 2016,
Accepted 20 Dec 2016

Keywords
- ✓ Mild steel,
- ✓ Hydrochloric acid,
- ✓ Corrosion inhibition,
- ✓ Adsorption,
- ✓ EIS

Latifa.elhattabi@gmail.com
Phone: +212687879263

Abstract

The 1-ethyl-1H-pyrazolo [3, 4-d] pyrimidine-4(5H)-thione (ETPP) has been evaluated as corrosion inhibitor for mild steel in 1M HCl solution by means of potentiodynamic polarization and electrochemical impedance spectroscopic measurements. The obtained results revealed that this compound is a good mixed type inhibitor with cathodic predominance effectiveness. The effect of temperature on the corrosion behavior with the addition of optimal concentration of 10^{-3}M was studied in temperature range of 303-343 K. The value of inhibition efficiency decreases slightly with the increasing of temperature. The adsorption of the inhibitor on the mild steel (MS) surface follows the Langmuir adsorption isotherm, indicating monolayer adsorption. The activation parameters indicate the inhibitor is physically adsorbed. The findings concerning the quantum chemical calculation indicate a high feasibility of molecular adsorption of ETPP.

1. Introduction

Corrosion problem occurs in many industries and can cause serious damages to metal and alloy in the system components causing economic consequences in terms of repair, replacement and product losses. Among various methods of metals corrosion protection, the use of inhibitors is most effective, economical and practical to prevent metals against electrochemical corrosion. The use of organic inhibitors to prevent the metal corrosion stands as an alternative method in industrial applications [1]. Acid solutions are generally used for removal of undesirable scale in the cleaning of boilers, heat exchangers, oil-well acidizing in oil recovery… [2,3]. Various inhibitors have been used to prevent dissolution of metals due to the corrosion [4-14]. The inhibitors are usually characterized by their ability of adsorption onto the metal surface through a strong metal-inhibitor interfacial interaction; these interactions depend on the molecule structure of the inhibitor [15,16]. Earlier studies have shown that organic compounds bearing heteroatom's with high electron density such as phosphorus, sulfur, nitrogen, oxygen or those containing multiple bonds, which are considered as adsorption centers, are effective inhibitors for the corrosion of metals [17-19]. The organic inhibitors are generally adsorbed on the metal surface through physical or chemical adsorption, which reduce the reaction area susceptible to corrosive attack [20,21].

This work aimed to determine the inhibitory features of 1-ethyl-1H-pyrazolo [3, 4-d] pyrimidine-4(5H)-thione on the mild steel (MS) surface using some electrochemical techniques. We studied the inhibitory efficiency and the adsorption type of 1-ethyl-1H-pyrazolo [3, 4-d] pyrimidine-4(5H)-thione on the mild steel corrosion, the effect of temperature and the concentration were also investigated.

2. **Experimental details**

2.1. *Synthesis of inhibitors*

The general strategy for the synthesis of 1-ethyl-1H-pyrazolo [3, 4-d] pyrimidine-4(5H)-thione is shown in Fig 1. A mixture of (0.54 g, 3.04 mmol) of 1-ethyl-pyrazolo [3, 4 - d] pyrimidin-4 (5H)-one and (0.84 g, 3.65 mmol) of phosphorus pentasulfide was refluxed in pyridine for 4h. Then the solvent is evaporated under reduced pressure; the formed precipitate is washed with hot water and recrystallized from ethanol solution to afford the wanted compound as yellow blocks. The product obtained was characterized by 1 H NMR, 13 C, IR and mass spectroscopy [22].

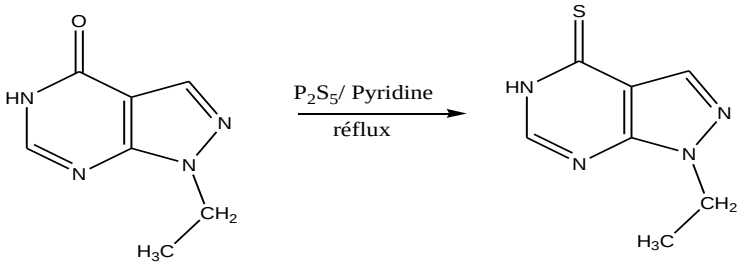

Figure 1: General reaction synthesis of 1-ethyl-1H-pyrazolo [3, 4-d] pyrimidine-4(5H)-thione

2.2 *Materials*

The steel used in this study is a carbon steel (mild steel) with a chemical composition (in wt%) of 0.370% C, 0.230% Si, 0.680% Mn, 0.016% S, 0.077% Cr, 0.011% Ti, 0.059% Ni, 0.009% Co, 0.160% Cu and the remainder iron (Fe). The surface area of the steel exposed to the test solution was $1cm^2$. Before the measurements, the surface of mild steel was mechanically abraded using different grades of SiC papers, which ended up with the 1200 grade. Then, the electrode was cleaned by washing with distilled water, acetone and distilled water, respectively and quickly immersed into the test solution.

2.3 *Test solutions*

The aggressive solutions of 1 M HCl were prepared by dilution of analytical grade 37% HCl with distilled water. The organic compound tested is 1-ethyl-1H-pyrazolo [3,4 d] pyrimidine-4(5H)-thione whose chemical structure is given in Fig 2. The electrochemical tests were carried out under air atmosphere without stirring the solutions. The temperature of the solutions was controlled thermostatically. The corrosion tests were performed in 1M HCl solution in the absence and presence of various concentrations (10^{-6}, 10^{-5}, 10^{-4} and 10^{-3} M) of 1-ethyl-1H-pyrazolo [3, 4-d] pyrimidine-4(5H)-thione.

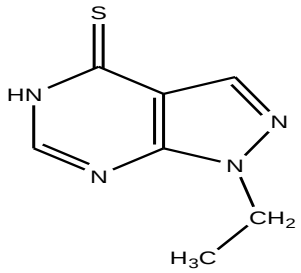

Figure 2: The chemical structure of the studied 1-ethyl-1H-pyrazolo[3, 4-d]pyrimidine-4(5H)-thione

2.4 *Electrochemical impedance spectroscopy (EIS)*

The electrochemical measurements were carried out using voltalab PGZ301. For these tests, an electrochemical cell with three-electrode configuration was used: platinum counter electrode, saturated calomel electrode as reference electrode and test material (mild steel) as working electrode. All potentials are reported versus saturated calomel electrode (SCE), and the measurements were done after 30 min of immersion in the test solution. Electrochemical impedance spectroscopy measurements were performed with a frequency range of 100 kHz-10 mHz and amplitude of 10 mV. The percentage inhibition efficiency (IE%) was calculated using the polarization resistance as follows:

$$IE\% = \left(1 - \frac{R_{ct_{blanc}}}{R_{ct_{inh}}}\right) \times 100 \qquad \textbf{(1)}$$

where ($R_{ct\ blanc}$) and ($R_{ct\ inh}$) are respectively charge transfer resistances in the absence and presence of inhibitor.

2.5. *Potentiodynamic polarization*

In potentiodynamic polarization study, polarization curves were recorded from -800 to -100 mV with respect to corrosion potential at a scan rate of 1 mV/s. The linear Tafel segments of the cathodic curves and the calculated anodic Tafel lines were extrapolated to the point of intersection to obtain the corrosion potential (E_{corr}) and corrosion current density (I_{corr}). The value of anodic Tafel slope (βa) and the cathodic Tafel slope (βc) were determined from experimental curves. The inhibition efficiency has been calculated by using respective corrosion current densities ($i°_{corr}$) and $(i°'_{corr})_{inh}$ in Eq, (2).

$$IE\% = \left(1 - \frac{i°'_{corr}}{i°_{corr}}\right) x100 \qquad \textbf{(2)}$$

where ($i°_{corr}$) and $(i°'_{corr})_{inh}$ are respectively the corrosion current densities ($\mu A/cm^2$) in the absence and presence of the inhibitor.

2.6. *Theoretical study*

All calculations were made by the method of density functional theory DFT / B3LYP (Becke-3-settings-Lee-Yang-Parr) with the base 6-311 ++ G (d. p). This method is implemented in the Gaussian 09 program, load analysis was conducted using the approach NBO (Natural Bond Orbital). The geometry of the molecule have been optimized in the calculation B3LYP / 6-311 ++ G (d. p) using the Gaussian 09 program. Recently, Density functional theory (DFT) has been used to analyse the characteristics of the inhibitor surface mechanism and to describe the structural nature of the inhibitor in the corrosion process [23,24]. Furthermore, DFT is considered a very useful technique to probe the inhibitor/surface interaction as well as to analyse the experimental data. This technique has been found to be successful in providing insights into the chemical reactivity and selectivity in terms of global parameters such as E_{HOMO}, E_{LUMO}, E_{HOMO} - E_{LUMO} energy gap (ΔE), electro-negativity (β), global hardness (γ), fraction of electrons transferred (ΔN) and Mulliken charges. To obtain detailed information about the inhibition mechanism, quantum theoretical calculations were performed and compared with the experimental results.

3. **Results and discussion**

3.1. *Characterization of inhibitor*

Inhibitor 1-ethyl-1H-pyrazolo [3, 4-d] pyrimidin-4 (5H) -thione is synthesized as a yellow solid with a yield of 75%. The compound was characterised by N.M.R and RX. **^{1}H-NMR** (DMSO-d6) (δ ppm): 14.03(s, 1H, NH), 8.04(s, 1H, CH), 8.39(s, 1H, CH), 1.22 (3H, t, J=7.2Hz. CH3); 3.96 (2H, q, J=7.2Hz, CH2); **^{13}C-NMR** (DMSO-d6) (δ ppm): 15.26(CH3), N1CH2 (42.29), 134.55 (=CH), 150.47 (=CH), Cq: 105.53, 151.20, 156.79.

IR: λ = 1100 cm^{-1}**, Mass Spectrum** (IE) M+ (m/z) = 180.

An X-ray crystallographic study of a single crystal of ETPP, figure 3 confirmed the structure deduced from NMR spectroscopic studies.

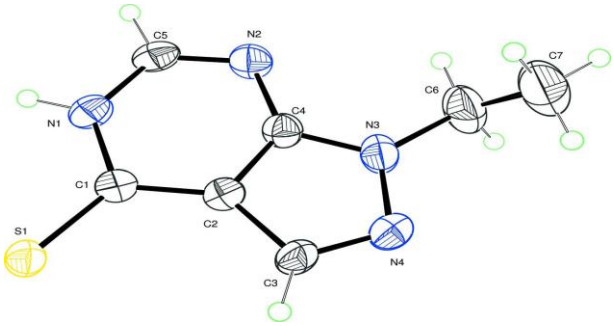

Figure 3: An ORTEP presentation of compound ETPP

3.2. *Potentiodynamic polarization measurements*

The representative potentiodynamic polarization curves of the mild steel electrode, which were obtained in 1M HCl solution in the absence and presence of various concentrations of ETPP, are given in fig. 4.

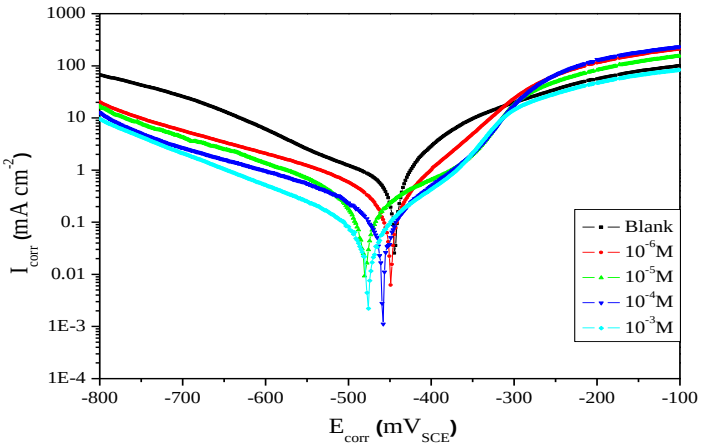

Figure 4: Polarization curves of mild steel in 1M HCl solution in the absence (blank) and presence of ETPP at 303 K

As known, cathodic and anodic regions correspond to hydrogen evolution and iron dissolution reactions under the experimental conditions, respectively, the figure 4 revealed that, the I_{corr} values decrease in the presence of different concentrations of ETPP, this can be explained by the fact that the anodic metal dissolution of iron and cathodic hydrogen evolution reaction were inhibited after the addition of ETPP to the acid solution 1M HCl [25, 26]. The cathodic current-potential curves (Fig. 4) are giving rise to parallel lines. The reduction of H^+ ions at the mild steel surface take place mainly through a charge transfer mechanism [27,28]. In order to obtain information about the kinetics of the corrosion, some electrochemical parameters, corrosion potential (E_{corr}), corrosion current density (I_{corr}), cathodic Tafel slopes (βc), anodic Tafel slopes (βa) and inhibition efficiency (IE %) values were calculated from the polarization curves by extrapolation method [29]; the obtained data are given in Table 1.

Table 1: Potentiodynamic polarization parameters for mild steel in 1M HCl in the absence and presence of different concentrations of ETPP

Concentration (M)	**$-E_{corr}$ (mV_{SCE})**	**I_{corr} ($\mu A\ cm^{-2}$)**	**β_a ($mV\ dec^{-1}$)**	**$-\beta_c$ ($mV\ dec^{-1}$)**	**IE (%)**	**θ**
Blank	444	523.55	167	142.7	--	--
10^{-6}	449	177.54	148.9	124.2	66	0.66
10^{-5}	479	148.71	146.3	168.2	72	0.72
10^{-4}	458	97.36	209.6	142.3	81	0.81
10^{-3}	476	58.28	230.2	240	89	0.89

Table1 shows that the increase in ETPP concentration increase of inhibition efficiency values that reach the maximum at concentration of 10^{-3} M at 303 K. The cathodic Tafel slope (βc) show slight changes with the addition of ETPP, which suggests that the inhibiting action occurred by simple blocking of the available cathodic sites on the metal surface, which lead to a decrease in the exposed area necessary for hydrogen evolution. It is reported in the literature that, if the displacement in E_{corr} is > 85 mV with respect to E_{corr} (blank), the inhibitor can be seen as a cathodic or anodic type and if displacement in E_{corr} is < 85, the inhibitor can be seen as mixed type. In the present study, shift in E_{corr} values is in the range of 5-35 mV, suggesting that meaning that this molecule (ETPP) could be classified as a mixed-type inhibitor with cathodic predominance (figure 4) [30].
From these results, ETPP prevent the carbon steel corrosion by blocking the reaction sites effectively. Similar results for aromatic pyrimidin derivates were reported in literature for example inhibition efficiency of 3-pyridinecarboxaldehyde thiosemicarbazone (3-PCT) on mild steel in 1M HCl achieved 88% [31], inhibition

efficiency increases with increasing concentration of bis-2,6-(3, 5-dimethylpyrazolyl) pyridine on the mild steel in HCl solution is reached 92% at 2.5×10^{-3} M [32].

3.3. Electrochemical impedance spectroscopy

Electrochemical impedance spectroscopy was used to determine the behavior of metal/solution interface in the absence and in the presence of inhibitor. The representative Nyquist plots of the mild steel electrode, which was obtained in 1M HCl solution in the absence and presence of various concentrations of ETPP, are shown in Fig 5. The Nyquist plots of mild steel in absence and presence of the inhibitor have a semi-circular shape and the diameter of semi-circle increases with increasing concentration of the inhibitor (figure 5) which indicates that the corrosion of mild steel in 1M HCl solution is mainly controlled by a charge transfer process [33-35].

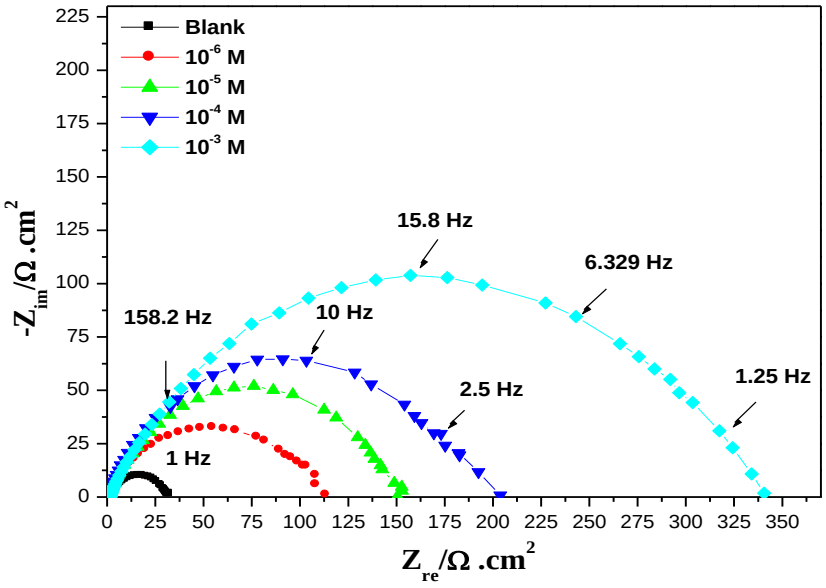

Figure 5: Nyquist diagrams for mild steel electrode in 1M HCl with and without ETPP after 30 min of immersion at 303 K

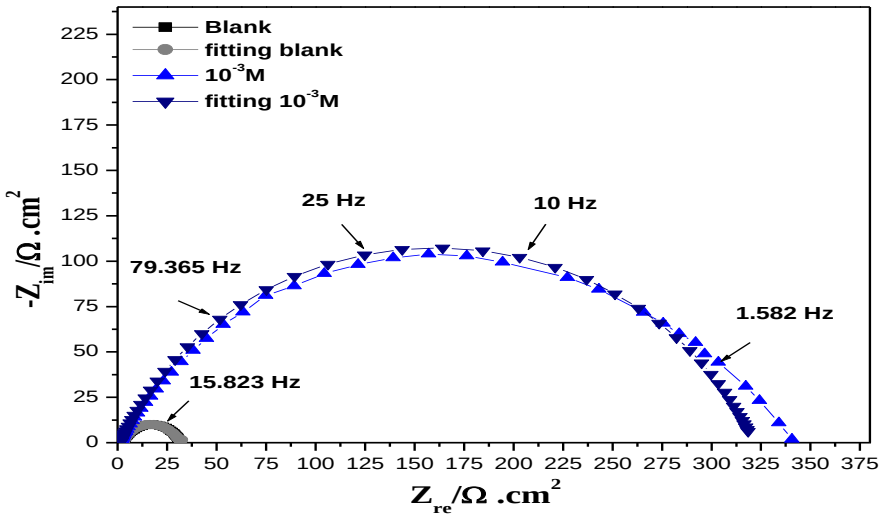

Figure 6: Fitting results the blank and optimal concentration obtained by Ec-Lab software

The experimental data were exploit by Ec-Lab software, and an electrical equivalent-circuit diagram corresponds to the metal/ solution interface was proposed (Figure 7). The obtained data are given in Table 2.

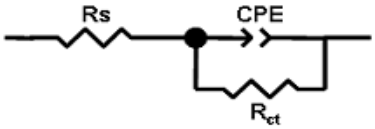

Figure 7: The equivalent circuit used to fit impedance spectra (Rs: solution resistance; Rct: charge transfer resistance; CPE: constant phase element)

Table 2: Electrochemical impedance parameters for mild steel in 1M HCl in the absence and presence of different concentrations of ETPP

	Concentration (M)	R_s ($\Omega.cm^2$)	R_{ct} ($\Omega.cm^2$)	f_{max} (Hz)	C_{dl} ($\mu F/cm^2$)	IE (%)
Blank	—	2.525	29.31	31.65	171.56	—
ETPP	10^{-6}	0.817	105	15.82	95.83	72
	10^{-5}	1.221	147.7	15.82	68.12	80
	10^{-4}	0.347	191.3	12.50	66.58	85
	10^{-3}	1.413	319.7	15.82	31.47	91

The increase in the value of R_{ct} with increasing concentration of the inhibitor ETPP (Table 2) indicates that the inhibitor molecules are adsorbed on the metal surface and inhibits the corrosion of mild steel [36]. Values of the double-layer capacitance C_{dl} were calculated from the frequency at which the impedance imaginary component $-Z_{im}$ is maximum using the equation:

$$f(-Zi_{\max}) = \frac{1}{2\pi.C_{dl}.R_{ct}} \qquad (3)$$

The increase in R_{ct} values can be attributed to the formation of protective film on the metal/ solution interface. The decrease in the C_{dl} values may be due to decrease in the local dielectric constant or an increase in the thickness of the electrical double layer. indicating that the inhibitor is adsorbed on the metal surface [37,38], also inhibition efficiency increase may be due to the gradual replacement of water by the ETPP molecules absorbed on the metal surface, decreasing the extent of dissolution reaction [39,40]. These results are similar to those obtained in the literature, Hammouti et al. [41] have measured the behaviors of inhibition of two organic compounds pyridine (P1) and pyrazole (P2) in acidic solution, the inhibition efficiencies increased with the increase in inhibitor concentration and reached 90% and 80% respectively for P1 and P2 in 1M HCl solution. Xiao-Ci et al [42] carried out the quantum chemical study of the corrosion inhibition effects of pyridine and its derivates at the aluminum electrode in HCl media the results showed that, the compounds is adsorbed in their protonated forms on the metal surface.

3.3. *Effect of temperature*

The temperature is an accelerating factor in most of chemical reactions. It increases the energy of the reacted species, as a result, chemical reactions get much faster. The corrosion reaction is a chemical reaction in which the Fe atoms at the metal surface react with the negatively charged anions (OH^-, SO_4^{2-}, Cl^-...). Hence, increasing the temperature of the environment increases the activation energy of the Fe atoms at the metal surface and accelerates the corrosion process of the carbon steel in the acidic media [43]. The effect of temperature on the corrosion behavior of steel in 1M HCl without and with inhibitor at a concentration 10^{-3} M is studied in the temperature range 303-343 K using the electrochemical measures. The results are presented in figures 8 and 9; the data of corrosion rates and corresponding efficiency collected from the two figures are presented in Table 3. Examination of table 3 revealed that the R_{ct} decreases in acid solution with the rise of temperature in the absence and presence of inhibitor. Inhibition efficiency values decreases with increase of temperature; we find 91% as inhibition efficiency value at 303 K and 78% at 343K.

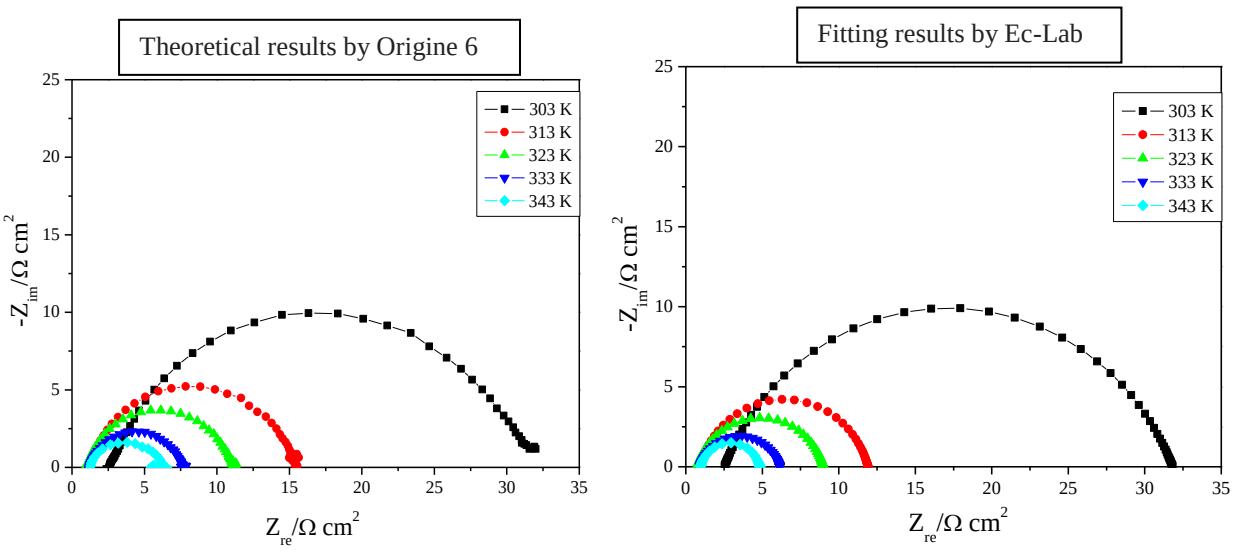

Figure 8: Nyquist diagrams for mild steel in 1 M HCl at different temperatures

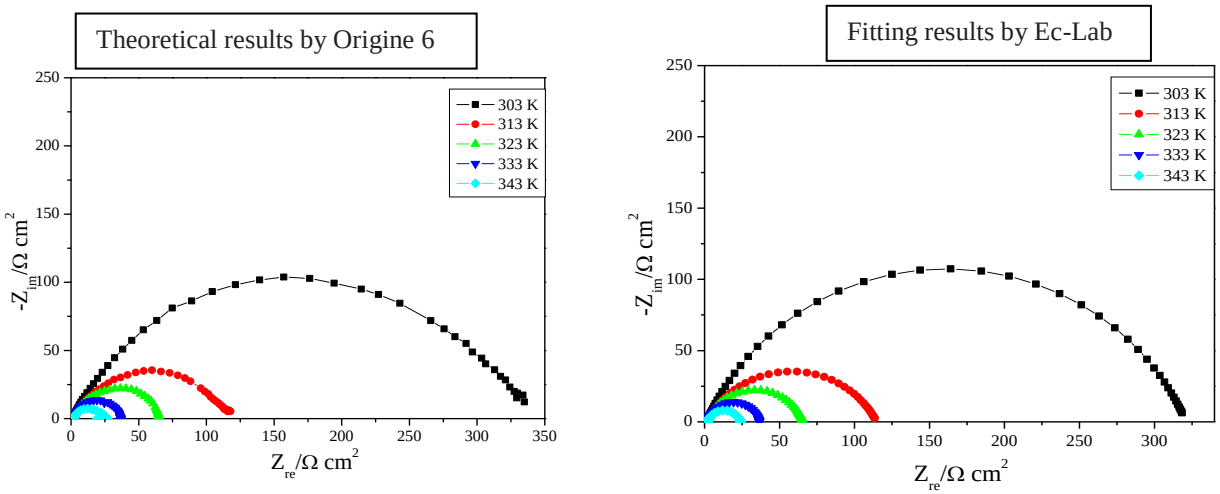

Figure 9: Nyquist diagrams for mild steel in 1M HCl + 10^{-3} M of ETPP at different temperatures

Table 3: Polarization resistance values and inhibition efficiencies obtained in 1M HCl in the absence and presence of 10^{-3} M concentration the ETPP in the different temperature

	ETPP			Blank	
T (K)	R_s (Ω cm^2)	R_{ct} (Ω cm^2)	IE (%)	R_s (Ω cm^2)	R_{ct} (Ω cm^2)
303	1.41	319.70	91	2.52	29.31
313	1.66	113.00	88	1.17	13.72
323	1.82	63.88	84	0.94	10.32
333	1.22	34.49	81	1.16	6.52
343	1.86	22.16	78	1.19	4.86

In the studied temperature range (303-343 K) the I_{corr} values obtained at the highest ETPP concentration, increase with increasing temperature, and the values of the inhibition efficiency of ETPP. The obtained results from impedance were in a good agreement with the ones obtained from polarization data (Table 4).

Table 4: Potentiodynamic polarization parameters for mild steel in 1M HCl in the absence and presence of 10^{-3} M concentration the ETPP in the different temperature

	Blank			ETPP	
T (K)	$-E_{corr}$ (mV_{SCE})	I_{corr} ($\mu A\ cm^{-2}$)	IE (%)	E_{corr} (mV_{SCE})	I_{corr} ($\mu A\ cm^{-2}$)
303	444.13	523.55	89	-475.64	58.28
313	469.07	1317.61	81	-475.44	246.40
323	455.13	2177.94	80	-490.80	439.64
333	556.22	3577.53	78	-413.79	773.36
343	457.37	4696.05	62	-490.80	1785.12

The maximum corrosion rate and the minimum inhibition efficiencies are reached at 343 K. In examining the effect of temperature on the corrosion of carbon steel, the activation parameters for the corrosion process were calculated from Arrhenius type plot according to the following equation [44]:

$$I_{corr} = A\exp\left(-\frac{E_a}{RT}\right) \qquad (4)$$

Where I_{corr} is corrosion current, A is a constant, T is the temperature, E_a is the apparent activation energy and R the universal gas constant. The variations of Ln (Icorr/T) and Ln (Icorr) against 1/T are presented in Figures 10 and 11. Enthalpy and entropy of activation were calculated using the alternative form of Arrhenius equation (5):

$$I_{corr} = \frac{RT}{Nh}\exp\left(\frac{\Delta S_a}{R}\right)\exp\left(\frac{\Delta H_a}{RT}\right) \qquad (5)$$

Where I_{corr} is corrosion current, h is Planck's constant and N is Avogadro's number, R is the universal gas constant. ΔH_a is the enthalpy of activation and ΔS_a is the entropy of activation. Figure 9 shows the plot of Ln (I_{corr}/T) versus 1/T. Straight lines were obtained with a slope of and an intercept of (Ln(R/Nh) + (ΔS_a /R) from which the values of ΔH_a and ΔS_a were calculated, and are listed in Table 5.

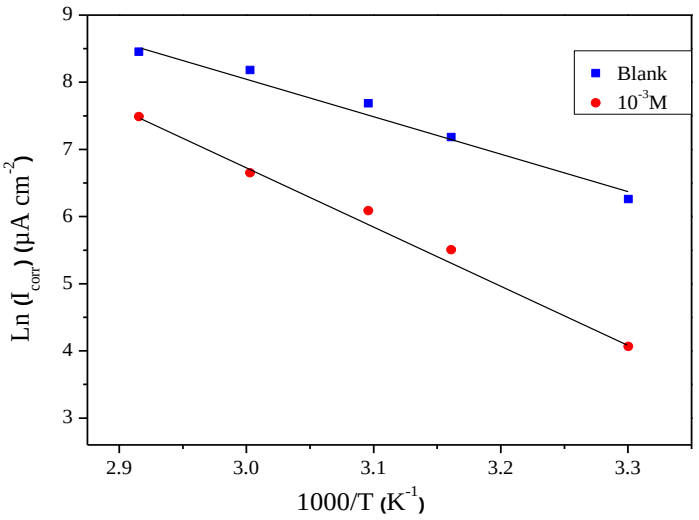

Figure 10: Arrhenius plots of mild steel in 1M HCl with and without 10^{-3} M of ETPP.

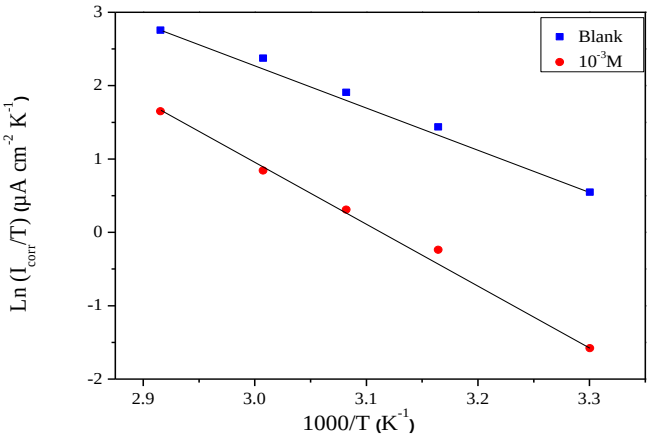

Figure 11: Transition Arrhenius plots of mild steel in 1M HCl with and without 10^{-3} M of ETPP.

Table 5: The values of activation parameters for mild steel in 1M HCl in the absence and presence of 10^{-3} M of ETPP

	E_a (kJ/mol)	ΔH_a (kJ/mol)	ΔS_a (J/mol K)
Blank	48.55	48.32	-33.03
ETPP	72.11	68.16	14.97

From Table 5, it seems that E_a and ΔH_a varied in the same way. The value of the activation energy for the corrosion process of the carbon steel in absence of the inhibitor is 48,55 kJ mol^{-1}, and E_a value are 72, 11 kJ mol^{-1} in presence of the ETPP. The used inhibitor increases the activation energy of the corrosion process due to their adsorption onto the metal surface [45]. It was found that, the presence of inhibitor shows higher value of ΔH_a than the obtained for the uninhibited solution indicating higher efficiency protection. This may be attributed to the presence of an energy barrier for the reaction. The positive signs of enthalpies (ΔHa) reflect the endothermic nature of dissolution process [46]. The value of ΔS_a is higher for the inhibited solution than that for the uninhibited solution. This suggests the formation of an ordered stable layer of inhibitor on the steel surface [47].

3.2. *Adsorption isotherm and thermodynamic parameters*

Adsorption isotherms are very important in understanding the mechanism of organo-electrochemical reactions. The most frequently used isotherms are Langmuir [48], Frumkin [49] and Temkin [50]. The Langmuir isotherm (C/θ vs. C) assumes that there is no interaction between adsorbed molecules on the surface. The Frumkin adsorption isotherm (θ vs. C) assumes that there is some interaction between the adsorbents, and the Temkin adsorption isotherm (θ vs. log C) represents the effect of multiple layer coverage [51]. In this study the best fit was determined with the use of the Langmuir adsorption isotherm (figure 12). It is represented by the following equation [52]:

$$\frac{C}{\theta} = \frac{1}{K_{ads}} + C \qquad (6)$$

C_{inh} is the inhibitor concentration; θ is the fraction of the surface covered. K_{ads} is the equilibrium constant for the adsorption–desorption process.

A straight line is obtained upon plotting C_{inh}/θ vs. C_{inh}, as given in Fig. 12. The linear correlation coefficient (R^2) is equivalent to 1 ($R^2 = 0.9999$) and slope is nearly 1, indicating that the ETPP compound adsorption on the surface of mild steel obeys Langmuir adsorption isotherm at 1 M HCl medium. The strong correlation to the isotherm of Langmuir adsorption may prove the effectiveness of this application. The equilibrium constant for the adsorption

process from Langmuir adsorption isotherm model is related to the standard free energy of adsorption by the expression:

$$\Delta G^{\circ}_{ads} = -RT\,Ln\left(55.5K_{ads}\right) \qquad (7)$$

where R is the universal gas constant, T is the absolute temperature and the value of 55.5 is the concentration of water in solution (mol/L).

In general the values of ΔG°_{ads} around -20 kJ mol^{-1} or lower are indicates that the electrostatic interaction between inhibitor and the electrode surface (physisorption); those around -40 kJ mol^{-1} or higher involve charge sharing or transfer from the inhibitor to the metal surface to form a coordinate type of bond (chemisorption) [53,54]. The value calculated of ΔG°_{ads} is -21,488 kJ.mol^{-1}. The value of ΔG°_{ads} for ETPP was slightly inferior to -40 KJ.mol^{-1}, indicating that the adsorption mechanism of ETPP on mild steel surface is probably the combination of both physisorption and chemisorption process.

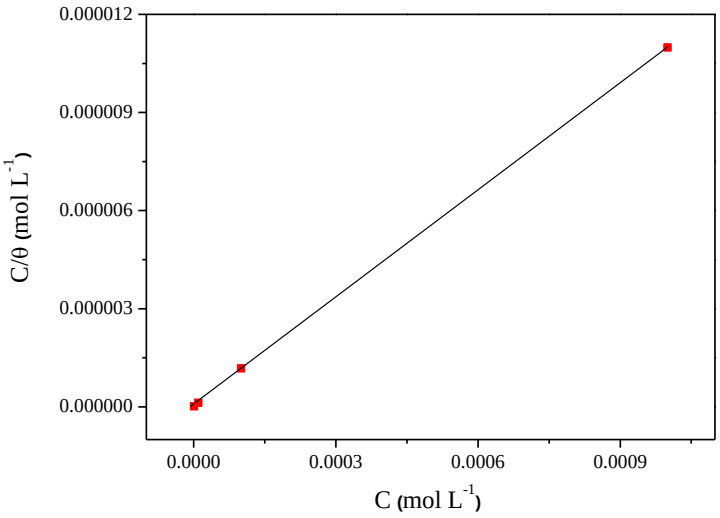

Figure 12: Langmuir adsorption plot of mild steel in 1M HCl solution containing different concentrations of ETPP.

3.3. *Theoretical calculations*

The fully optimized structure of ETPP molecule is given in Fig. 13. In order to construct a composite index of an inhibitor molecule it may be important to focus on parameters that directly influence the electronic interaction of the inhibitor molecules with the metal surface. These are mainly: energies of the molecular orbital. E_{HOMO}, E_{LUMO}, ΔE (E_{LUMO} - E_{HOMO}), dipole moment (μ) and total energy (TE).

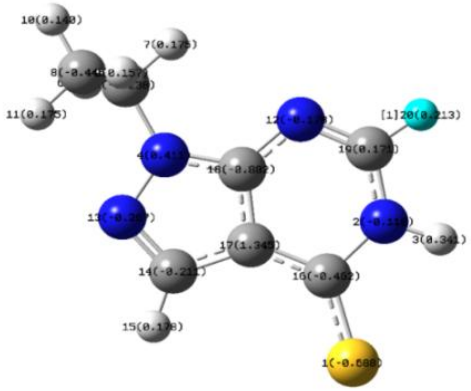

Figure 13: Optimised structures of ETPP

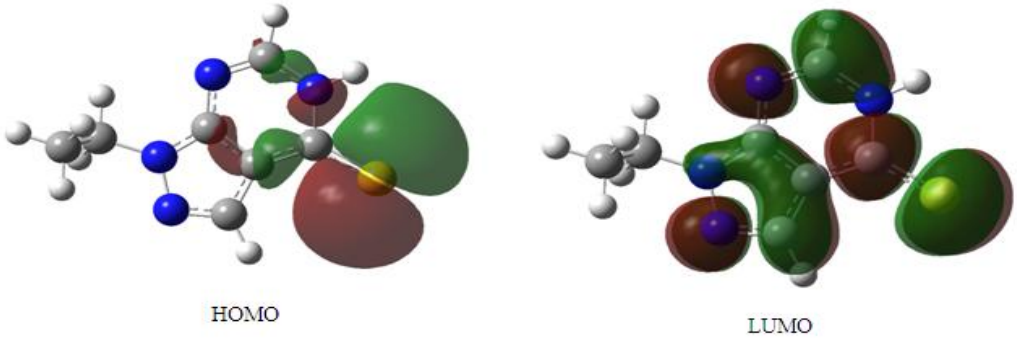

Figure 14: Frontier molecular orbital density distribution of ETPP

Analysis of Figure 14 shows the distribution of two energies HOMO and LUMO, we can see that the electron density of the HOMO and LUMO location was distributed almost within the entire molecule. The values of these calculated quantum chemical parameters are listed in Table 6. According to Wang et al. [55], the frontier orbital (highest occupied molecular orbital-HOMO and lowest unoccupied molecular orbital-LUMO) of a chemical species play major role in defining its reactivity. As E_{HOMO} is often associated with the electron donating ability of a molecule, high value of E_{HOMO} are likely to indicate the tendency of the molecule to donate electrons to appropriate acceptor molecules with lower energy MO. Increasing values of E_{HOMO} facilitate adsorption and therefore enhance the inhibition efficiency, by influencing the transport process through the adsorbed layer. E_{LUMO} indicates the ability of the molecule to accept electrons. The binding ability of the inhibitor to the metal surface increases with increasing of the HOMO and decreasing of the LUMO energy values. Apparently, excellent corrosion inhibitors are usually organic compounds which not only offer electrons to unoccupied orbital of the metal but also accept free electrons from the metal [56]. Generally, value of ΔN shows inhibition efficiency resulting from electron donation, and the inhibition efficiency increases with the increase in electron-donating ability to the metal surface. According to Lukovits's study [57], if $\Delta N < 3.6$, the inhibition efficiency increases with increasing electron-donating ability at the metal surface. Based on these calculations, it is expected that the synthesized inhibitor is donor of electrons and the steel surface is the acceptor, and this favorites' chemical adsorption of the inhibitor on the electrode surface. Here the inhibitor binds to the steel surface and forms an adsorption layer against corrosion.
For iron, the theoretical values of γ_{Fe} and β_{Fe} are 0 eV and 7 eV, respectively [58]. The values of β, γ and μ are also given in table 6. Some studies [58, 59] indicate that the β parameter is related to the chemical potential, where a higher value of β corresponds to better inhibition efficiency. Conversely, γ is equal to ΔE/2, and lower values of γ indicate higher polarizability and higher inhibitive achievement. Additionally, for the dipole moment (μ), higher value of μ will favor the interaction between the molecule and the surface of the substrate [60]

Table 6: Calculated quantum chemical parameters of the studied compound

Quantum parameters	**ETPP**
E_{HOMO} (eV)	-6.18
E_{LUMO} (eV)	-1.90
μ (debye)	4.7679
β (eV)	1.90
γ (eV)	2.14
ΔN	0.691
ΔE_{gap} (eV)	4.28

The Mulliken charge distribution of ETPP is presented in Table 7. It has been reported that as the Mulliken charges of the adsorbed center become more negative, the atom donates its electron more easily to the unoccupied orbital of the metal [61]. It could be readily observed that nitrogen, oxygen and some carbon atoms have high charge

densities. The regions of highest electron density are generally the sites to which electrophiles can attach [62]. Therefore, N, S and some C atoms are the active centers, which have the strongest ability to bond to the metal surface. Conversely, some carbon atoms carry positive charges, which are often sites where nucleophiles can attach. Therefore, ETPP can also accept electrons from Fe through these atoms. It has been reported that excellent corrosion inhibitors can not only offer electrons to unoccupied orbitals of the metal but also accept free electrons from the metal [63].

Table 7: Mulliken atomic charges of the ETPP molecule

Atom K	Charge de Mulliken
1 S	-0.688370
2 N	-0.109911
3 H	0.340746
4 N	0.411273
5 C	-0.237536
6 H	0.178093
7 H	0.174743
8 C	-0.446300
9 H	0.156645
10 H	0.139818
11 H	0.175245
12 N	-0.178444
13 N	-0.267418
14 C	-0.210873
15 H	0.178414
16 C	-0.462408
17 C	1.344897
18 C	-0.882440
19 C	0.170835
20 H	0.212989

Conclusion

In this study, 1-ethyl-1H-pyrazolo [3, 4-d] pyrimidine-4(5H)-thione (ETPP), was tested as corrosion inhibitor for carbon steel in 1 M HCl using polarization and electrochemical impedance spectroscopy (EIS) in the range of temperature 303-343 K. The inhibition efficiency increased with increasing in the inhibitor concentration, we find maximum efficiency of 91% for optimal concentration of 10^{-3}M. ETPP acted as a mixed-type inhibitor with cathodic predominance. The adsorption of ETPP on carbon steel surface obeys the Langmuir adsorption isotherm. The correlation between the quantum chemical parameters and inhibition efficiencies of ETPP was investigated using DFT calculations. The results the quantum chemical parameters such as ΔE (gap), EHOMO, ELUMO, dipole moment (μ) and ΔN show that there is a correlation between quantum and experimental parameters.

References

1. Ahamad I., Prasad R., Quraishi M.A., *Corros. Sci*. 52 (2010) 3033–3041.
2. Avdeev Y.G., Kuznetsov Y.I., Buryak A.K., *Corros. Sci*. 69 (2013) 50– 60.
3. Kardas G., *Mater. Sci*. 41 (2005) 337–343
4. Mert B.D., Mert M.E., Kardas G., Yazici B., *Corros. Sci*. 53 (2011) 4265–4272
5. Mahdavian M., Ashhari S., *Electrochim. Acta* 55 (2010) 1720–1724.
6. Zarrok H., Oudda H., El Midaoui A., Zarrouk A., Hammouti B., Ebn Touhami M., Attayibat A., Radi S., Touzani R., *Res. Chem. Intermed*. 38 (2012) 2051.

7. Zarrouk A., Hammouti B., Zarrok H., Bouachrine M., Khaled K.F., Al-Deyab S.S., *Int. J. Electrochem. Sci*. 6 (2012) 89.
8. Zarrouk A., Hammouti B., Dafali A., Zarrok H., *Der Pharm.Chem*. 3 (4) (2011) 266.
9. Zarrok H., Zarrouk A., Salghi R., Oudda H., Hammouti B., Assouag M., Taleb M., Ebn Touhami M., Bouachrine M., Boukhris S., *J. Chem. Pharm. Res*. 4 (2012) 5056.
10. Ghazoui A., Zarrouk A., Bencaht N., Salghi R., Assouag M., El Hezzat M., Guenbour A., Hammouti B., *J. Chem. Pharm. Res*. 6 (2014) 704
11. Zarrok H., Zarrouk A., Salghi R., Assouag M., Hammouti B., Oudda H., Boukhris S., Al Deyab S.S., Warad I., *Der Pharm. Lett*. 5 (2013) 43.
12. Belayachi M., Serrar H., Zarrok H., El Assyry A., Zarrouk A., Oudda H., Boukhris S., Hammouti B., Ebenso Eno E., Geunbour A., *Int. J. Electrochem. Sci*. 10 (2015) 3010.
13. Zarrouk A., Zarrok H., Salghi R., Touir R., Hammouti B., Benchat N., Afrine L.L., Hannache H., El Hezzat M., Bouachrine M., *J. Chem. Pharm. Res*. 5 (2013) 1482.
14. Zarrok H., Zarrouk A., Salghi R., Ebn Touhami M., Oudda H., Hammouti B., Touir R., Bentiss F., Al-Deyab S.S., *Int. J. Electrochem. Sci*. 8 (2013) 6014.
15. Döner A., Solmaz R., Özcan M., Kardas G., *Corros. Sci*. 53 (2011) 2902–2913.
16. Tao Z., Zhang S., Li W., Hou B., *Ind. Eng. Chem. Res*. 49 (2010) 2593–2599.
17. Solmaz R., Altunbas E., Kardas G., *Prot. Met. Phys. Met*. 47 (2011) 262–269.
18. Farag A.A., Ali T.A., *J. Ind. Eng. Chem*. 21 (2015) 627–634.
19. Bouanis F.Z., Bentiss F., Traisnel M., Jama C., *Electrochim. Acta*. 54 (2009) 2371.
20. Obot I.B., Obi-Egbedi N.O., Umoren S.A., *Corros. Sci*. 51 (2009) 1868–1875.
21. Mar L., Xometl O., Aguilar M., Flores E., Lozada P., Cruz F., *Corros. Sci*. 61 (2012) 171–184.
22. El Fal M., Ramli Y., Essassi E.M., Saadi M., El Ammari L., *Acta Cryst*. 70 (2014) 1005-1006.
23. Valdez L.R., Villafane A.M., Mitnik D.G., *J. Mol. Struct*. 61 (2005) 716.
24. Lashkari M., Arshadi M.R., *Chem. Phys*., 299 (2004) 131-137.
25. Khaled K.F., Jackerman N., *Electrochim. Acta* 48 (2003) 2715.
26. Hegazy M.A., Badawi A.M., Abd El Rehim S.S., Kamel W.M., *Corros. Sci*. 69 (2013) 110.
27. Lebrini M., Lagrenee M., Vezin H., Gengembre L., Bentiss F., *Corros. Sci*. 47 (2005) 485.
28. Li L., Zhang X., Lei J., He J., Zhang S., Pan F., *Corros. Sci*. 63 (2012) 82.
29. Zarrok H., Zarrouk A., Hammouti B., Salghi R., Jama C., Bentiss F., *Corros. Sci.* 64 (2012) 243.
30. Ferreira E.S., Giancomelli C., Giacomelli F.C., Spinelli A., *Mater. Chem. Phys.* 83 (2004) 129.
31. Xu B., Liu Y., Yin X., Yang W., Chen Y., *Corros. Sci*. 74 (2013) 206–213.
32. Egurn Ü., Yüzer D., Emregül K.C., *Materials Chemistry and Physics*. 109 (2008) 492–499.
33. Zhang Q.B., Hua Y.X., *Electrochim. Acta* 54 (2009) 1881–1887.
34. Touhami F., Aouniti A., Abed Y., Hammouti B., Kertit S., Ramdani A., Elkacemi K., *Corros. Sci*. 42 (2000) 929–940.
35. El Achouri M., Kertit S., Gouttaya H.M., Nciri B., Bensouda Y., Perez L., Infante M.R., Elkacemi K., *Prog. Org. Coat*. 43 (2001) 267–273.
36. Singh A.K., Shukla S.K., Quraishi M.A., Ebenso E.E., *J .Chin .Inst .Chem .Eng* 43(2012) 463–72.
37. Prabhu R., Venkatesha V., Shanbhag V., Kulkarni G., Kalkhambkar R., *Corro. Sci* 50 (2008) 3356.
38. Tang Y., Yang X., Yang W., Chen Y., Wan R., *Corros . Sci* 52 (2010) 242.
39. Benali O., Larabi L., Mekelleche S.M., Harek Y., *J. Mater. Sci*. 41 (2006) 7064–7073.
40. Hackerman N., Snavely E.S., Payne J., *J. Electrochem. Soc.* 133 (1966) 677–681.
41. Tebbji K., Oudda H., Hammouti B., Benkaddour M., El Kodadi M., Ramdani A., *Eng. Aspects* 259 (2005) 143–149.
42. Xiao-Ci Y., Hong Z., Ming-Dao L., Hong-Xuan R., Lu-An Y., *Corros. Sci*. 42 (2000) 645–653
43. Negm N.A., Elkholy Y.M., Zahran M.K., Tawfik S.M., *Corros Sci*. 52 (*2010*) 3523–3536.
44. Dogru Mert B., Mert M.E., Kardas G., Yazıcı B., *Corros. Sci*. 53 (2011) 4265–4272
45. Negm N.A., Zaki M.F., Colloid Surf. A: Physicochem. *Eng. Aspec*. 322 (2008) 97–102.
46. Guan N.M., Xueming L., Fei L., *Mater. Chem. Phys.* 86 (2004) 59–68.
47. Yurt A., Balaban A., Kandemir S.U., Bereket G., Erk B., *Mater. Chem. Phys.* 85 (2004) 420-426.
48. Langmuir, I., *J. Am. Chem. Soc*. 39 (1947) 1848.
49. Frumkin, A.N.Z., *Phys. Chem*. 116 (1925) 466.

50. De Boer J.H., Kaspersma J.H., Van Dongen R.H., Broekhoff J.C.P., *Journal of Colloid and Interface Science*, 38 (1972) 97-100.
51. Masel R.I., *John Wiley & Sons.* 3 (1996).
52. Bockris J.O.M., Reddy A.K.N., Gamboa-Aldeco M., *Modern Electrochemistry 2A: Fundamentals of Electrodics*. (2000) 1455-1534.
53. Abd El-Lateef H.M., Abbasov V.M., Aliyeva L.I., Qasimov E.E., Ismayilov I.T., *Mater. Chem. Phys.* 142 (2013) 502–512.
54. Jevremovic I., Singer M., Nešic S., Stankovic V.M., *Corros. Sci*. 77 (2013) 265–272.
55. Wang H., Wang X., Wang H., Wang L., Liu A., *J. Mol. Model*. 13 (2007) 147.
56. Choa P., Liang Q., Li Y., *Appl. Surf. Sci*. 252 (2005) 1596.
57. Khaled K.F., *Appl. Surf. S*ci. 255 (2008) 1811.
58. El Adnani Z., Mcharfi M., Sfaira M., Benzakour M., Benjelloun A.T., Ebn Touhami M., *Corros. Sci.* 68 (2013) 223–230.
59. Ju H., Kai Z.P., Li Y., *Corros. Sci.* 50 (2008) 865–871.
60. Anejjar A., Zarrouk A., Salghi R., Ben Hmamou D., Zarrok H., Al-Deyab, M. Bouachrine S.S., Hammouti B., Benchat N., *Int. J. Electrochem. Sci.* 8 (2013) 5961 – 5979.
61. Lukovits I., Kalman E., Zucchi F., *Corrosion* 57 (2001) 3.
62. Xia S., Qiu M., Yu L., Liu F., Zhao H., *Corros. Sci*. 50 (2008) 2021.
63. Al-Amiery A.A., Musa A.Y., Kadhum A.A.H., Mohamad A., *Molecules*. 16 (2011) 6833.

(2017) ; http://www.jmaterenvironsci.com /